Column-loss response of RC beam-column sub-assemblages with different bar-cutoff patterns

Meng-Hao Tsai[*], Jun-Kai Lu[a] and Bo-Hong Huang[b]

*Department of Civil Engineering, National Pingtung University of Science and Technology,
No.1 Hseuh-Fu Rd., Neipu, Pingtung County, 912, Taiwan*

Abstract. Static loading tests were carried out in this study to investigate the effect of bar cutoff on the resistance of RC beam-column sub-assemblages under column loss. Two specimens were designed with continuous main reinforcement. Four others were designed with different types of bar cutoff in the mid-span and/or the beam-end regions. Compressive arch and tensile catenary responses of the specimens under gravitational loading were compared. Test results indicated that those specimens with approximately equal moment strength at the beam ends had similar peak loading resistance in the compressive arch phase but varied resistance degradation in the transition phase because of bar cutoff. The compressive bars terminated at one-third span could help to mitigate the degradation although they had minor contribution to the catenary action. Among those cutoff patterns, the *K*-type cutoff presented the best strength enhancement. It revealed that it is better to extend the steel bars beyond the mid-span before cutoff for the two-span beams bridging over a column vulnerable to sudden failure. For general cutoff patterns dominated by gravitational and seismic designs, they may be appropriately modified to minimize the influence of bar cutoff on the progressive collapse resistance.

Keywords: static loading test; column loss; bar cutoff; RC sub-assemblage; arch action; catenary action

1. Introduction

Development of practical and efficient approaches for protecting building structures from progressive collapse under accidental column loss has been an imperative issue in the past decade. Among several feasible measures proposed in the literatures (Abruzzo *et al*. 2006, Ellingwood 2006, Mohamed 2006, Nair 2006, Yagob *et al*. 2009, Almusallam *et al*. 2010), providing alternate load paths has become an acceptable and popular solution for reducing the failure risk under sudden column loss. Reliable alternate load paths usually depend on the integrity, redundancy, and strength of the remaining structural members. The two-span beams bridging over the failed column may be regarded as the most important role to redistribute loads. In conventional structural design and analysis, pure bending capacity has been used to define the flexural strength of beam

─────────────────

[*]Corresponding author, Professor, E-mail: mhtsai@mail.npust.edu.tw
[a]Professor, E-mail: julu@mail.npust.edu.tw
[b]Graduate Student, E-mail: we79818@yahoo.com.tw

members. Nevertheless, it is known that compressive arch and tensile catenary actions may be developed to resist the gravitational loading for appropriately restrained flexural members. Several analytical studies have been conducted to investigate the compressive arch and catenary behavior of flexural members. Guice and Rhomberg (1989) used a simple truss element model to simulate the compressive-to-tensile membrane behavior of restrained RC slabs. Three distinct regions, namely compressive membrane, transition, and tensile membrane, were observed from the slab elements under gravitational loading. Izzudin (2005) proposed a simplified explicit model for axially restrained beams subjected to extreme transverse loading. The elasto-plastic response of an axially restrained steel beam under transverse loading was divided into elastic, plastic bending, transient catenary, and final catenary stages in the model. Lee *et al*. (2009) adopted a steel sub-assemblage to evaluate the progressive collapse potential of welded steel frames. It was observed that the sectional moment capacity decreased with increasing catenary force. Similar analysis results were revealed by Kim and An (2009) and Liu (2010).

Recently, some experimental studies were conducted to investigate the column-loss response of RC frames. Yi *et al*. (2008) performed static load-release test on a one-third scaled three-story frame sustaining a concentrated loading. The test results revealed that the tested frame experienced distinct elastic, plastic, and catenary phases during the unloading process and eventually collapsed at a rotational angle around 10.3 degrees. Also, collapse resistance of the frame was conservatively estimated by using plastic limit analysis. Su *et al*. (2009) conducted static vertical loading tests on twelve longitudinally restrained RC beams with varied reinforcement ratios and span-to-depth ratios. The tested specimens generally reached peak compressive arch strength at a deflection ranging from 16% to 34% of section depth. The load resistance in catenary stage might be lower than the arch strength. Some experiments were conducted by using beam-column sub-assemblages. Sasani and Kropelnicki (2008) and Sasani *et al*. (2011) adopted a 3/8 scaled sub-assemblage to investigate the column-loss response of an RC beam bridging over the removed column. Full-scale steel and RC sub-assemblages were constructed and tested by Sadek *et al*. (2011) to examine the difference between the column-loss response of intermediate and special moment frames. Choi and Kim (2011) performed static loading tests on reduced-scale RC sub-assemblages designed with and without seismic detailing and concluded that significant catenary action may be activated for seismically detailed beams. Two one-half scaled assemblages were designed and tested by Yu and Tan (2011) to investigate the influence of seismic details on progressive collapse resistance. In addition to the above static loading experiments, dynamic column-loss tests were also carried out for prototype and reduced-scale specimens (Sasani and Sagiroglu 2010, Tian and Su 2013). From these evidences, it is recognized that experimental studies are important and necessary to clarify the column-loss response of various member details.

Depending on member deflection, the response of an RC beam-column sub-assemblage under monotonic loading may be generally divided into three regions, namely compressive arch, transition, and catenary regions. Major factors influencing the response in each individual region include the reinforcement ratio, span-to-depth ratio, and restraint stiffness of the two-span member bridging over the notional failed column. In design practice, flexural reinforcement of RC beams may be cut off at appropriate locations as long as the remaining steel bars are sufficient to provide required moment resistance. This makes the reinforcement ratio may vary along the spans. Hence, experimental investigation for the effect of bar cutoff on the column-loss response of RC members was performed in this study. Monotonic static loading tests on beam-column sub-assemblages designed with varied cutoff patterns were carried out. Four different types of cutoff were defined. Their test results were compared with two sub-assemblages with continuous bars to evaluate the
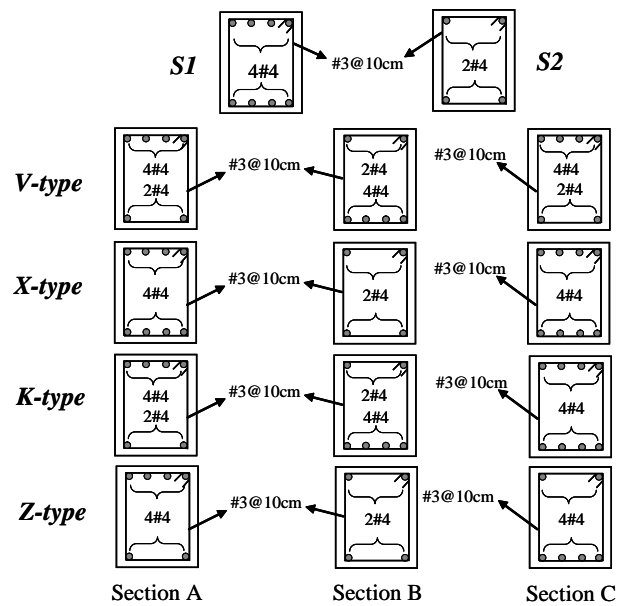
Fig. 1(a) Bar layout of test specimens

effect of bar cutoff on the column-loss behavior. Practical suggestions for minimizing the influence of bar cutoff on the progressive collapse resistance of RC members were provided.

2. Design of test specimens

2.1 Determination of dimensions

Dimensions of the test specimens were determined with reference to the design drawings of a real ten-story RC building frame (Tsai and Huang 2013). The peripheral beams of the frame had span-to-depth ratios varying from 5.0 to 10.3. Main reinforcement ratio at the beam-end sections of the second floor ranged from 0.82% to 1.64%. The beam-end reinforcement of some members was unsymmetrical with respect to the mid-span. The reinforcement ratios of most members were reduced to 0.61% at the mid-span region by terminating some steel bars at one-third span from the beam ends. Considering the available space for installation of test setup, the clear span of the beam-column specimens was determined as 1600 mm and the section dimensions were 200 mm in width and 250 mm in depth. This resulted in a span-to-depth ratio of 6.4. Also, since the purpose of this experiment was focused on the collapse resistance of the two-span beams, a larger section with 300 mm in width and 400 mm in depth was used for the end and middle column stubs.

2.2 Types of bar cutoff

As shown in Fig. 1(a), two standard specimens denoted as S1 and S2 were designed with continuous main reinforcement. The reinforcement ratios of S1 and S2 were equal to 1.21% and 0.61%, respectively, and regarded as strong and weak flexural design. Four other specimens were
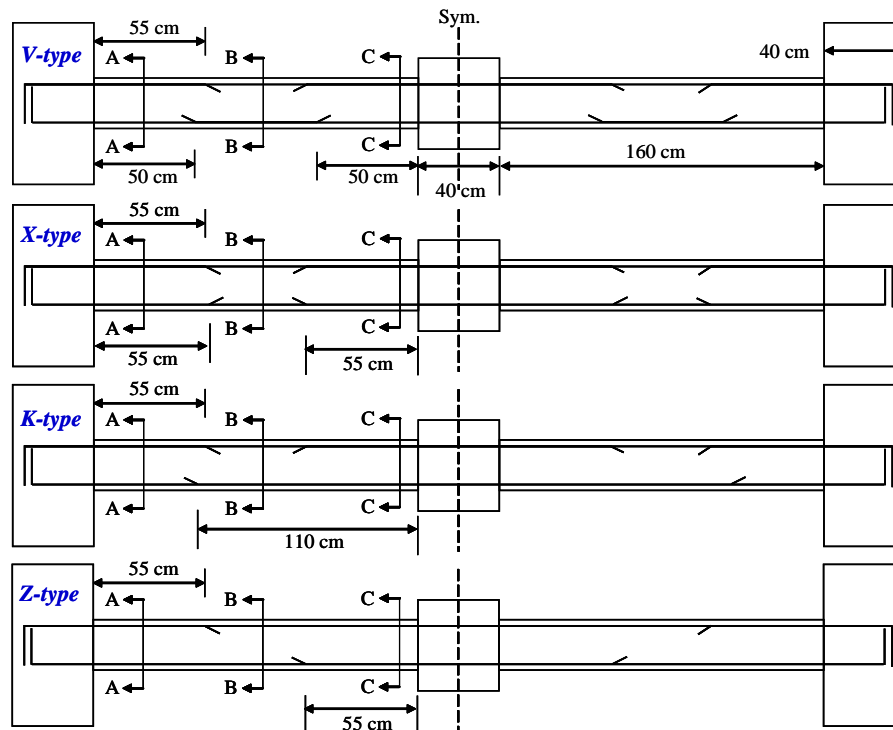
Fig. 1(b) Detailed bar cutoff locations

designed with bar cutoff at varied locations for comparisons. The detailed locations of cutoff and bar layouts are shown in Fig. 1(b) and 1(a), respectively. According to the cutoff pattern, they were designated as *V*-, *X*-, *K*-, and *Z*-type specimens. The *V*-type specimen represented a typical gravitational-controlled bar layout with cutoff of partial top bars at the mid-span and partial bottom bars at the beam-end regions. The *X*-type specimen on the other hand represented a typical seismic-controlled bar layout with cutoff of partial top and bottom bars at the mid-span region. The *K*-type was actually modified from the *V*-type with extending the terminated bottom bars into the middle joint for investigating its benefit on collapse resistance. The *Z*-type specimen was used as a strengthened case against progressive collapse for the weak flexural design S2. Also, the test results of the *Z*-, *X*- and *K*-type specimens could be compared to investigate the effect of the terminated compressive bars on loading resistance.

2.3 Material strength

Reinforcing steel bars of ASTM (American Society for Testing Materials) standard were adopted in the experiment. For the two-span beams, #4 steel bars were used as the main reinforcement and confined with #3 shear stirrups spaced at 100 mm. For the column stubs, ten #7 steel bars were used and confined with #5 shear stirrups spaced at 100 mm. Clear cover of concrete was 25 mm for both the beam and column sections. Design yield strength was 275 MPa for steel bars not larger than #5 and 412 MPa for #7. Design compressive strength of concrete was 20.6 MPa. Three standard concrete cylinders and three steel coupons of each bar size were tested

Table 1 Material test results for steel reinforcement

Bar #	σ_y (MPa)	ε_y (%)	σ_u (MPa)	ε_u (%)
3	340	0.20	490	16
4	360	0.20	550	13
5	360	0.27	540	16
7	466	0.43	663	13

Table 2 Beam-end yield moment and flexural yield load

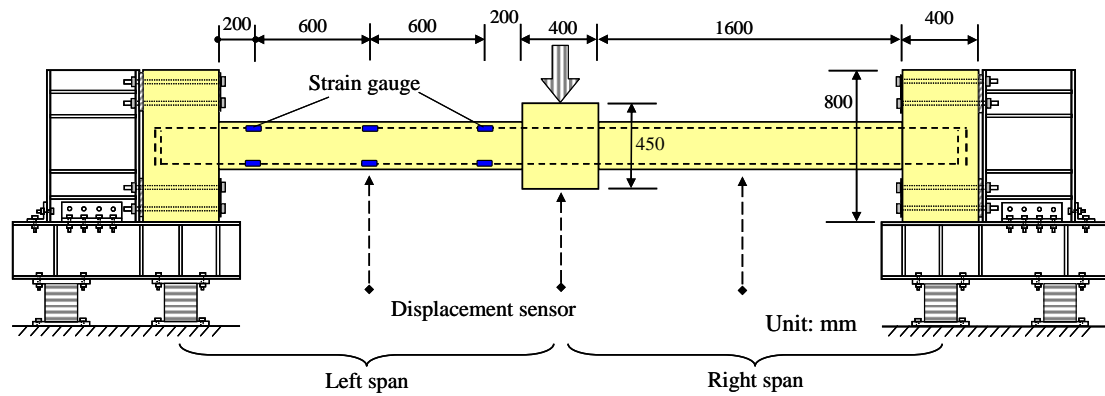| Specimen	M^-_y (kN-m)	M^+_y (kN-m)	P_y (kN)
S1	31.46	31.46	78.65
S2	16.26	16.26	40.65
V-type	31.12	15.90	58.78
X-type	31.46	31.46	78.65
K-type	31.12	31.46	78.23
Z-type	31.12	31.12	77.80

Fig. 2 Experimental setup and sensor arrangement

to identify the material strength. The compressive strength of concrete obtained from the cylinder tests was equal to 21.2 MPa, 22.2 MPa, and 23.2 MPa. They were approximately equal to the design value. However, test results of the steel coupons revealed apparently higher yield strength than the design value. The average yield and ultimate strength of the tested steel bars are tabulated in Table 1. The corresponding yield and ultimate strains (ε_y and ε_u) are also included in the table. Based on the material tests, the positive and negative yield moment at the interior and exterior beam ends, respectively denoted as M^+_y and M^-_y, are summarized in Table 2.

3. Test setup and test program

Fig. 2 shows a schematic drawing with dimensions of the test setup. The side column of specimen was bolted to a reaction seat made of H488×300 and H300×300 steel sections. The reaction seat was connected to the strong floor through two bi-axial load cells, which were used to

Fig. 3 A photo of the test setup

measure the horizontal and vertical reactions. A downward loading was imposed on the top of the middle column stub through a 1000 kN hydraulic actuator. The actuator was installed to a steel portal reaction frame. A typical picture of the test setup is shown in Fig. 3. The imposed load and displacement of the actuator were respectively measured by a built-in load cell and a displacement sensor. Displacement responses at the mid-span and the middle column stub were measured by position transducers. Also, twelve strain gauges were distributed in the left span of the sub-assemblage, as shown in Fig. 2.

At the beginning of each test, a plaster layer was cast on the top of the middle column stub. This was to assure that the column top may be fully in contact with the loading surface of actuator. The downward loading was then applied through displacement control to observe the response of the test specimen. It began at a loading rate of 0.25 mm/sec and was suspended as the deflection reached 10 mm, 20 mm, and 50 mm for labeling the crack propagation. After 50 mm, the loading rate was doubled and the displacement was increased steadily until the end of test. It was assumed that the deflection of the specimen could be gradually increased to fracture the tensile steel bars. However, due to safety consideration and restriction of the test facilities, the loading process might be terminated any time as the deflection exceeded 400 mm.

4. Test results

4.1 Damage and crack patterns

Figs. 4(a) and 4(b) present the ultimate deformed configurations of the S1 and S2 specimens, respectively. More serious damage to right span of S1 was observed because of an accidental inclination of the loading surface during the test. The test was terminated as the displacement reached 436 mm. After an appropriate adjustment, S2 displayed approximately symmetric damage to both spans. For the S1 specimen, flexural cracks originated from the beam ends and extended toward the mid-span in a sector shape. Different from that, several discrete flexural cracks formed amid the spans of S2. As shown by the local enlargement in Fig. 4(b), fracture of the top reinforcement at the exterior beam end of the right span occurred as the deflection reached 526 mm.

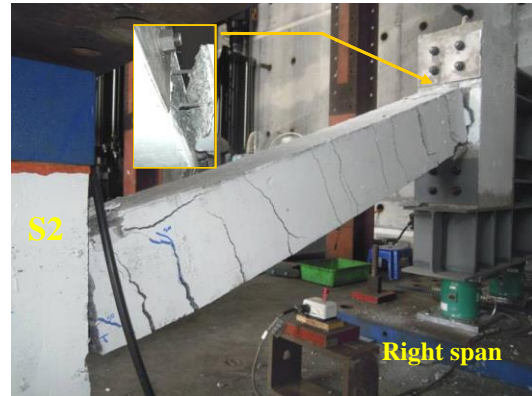Fig. 4(a) Damage configuration of S1
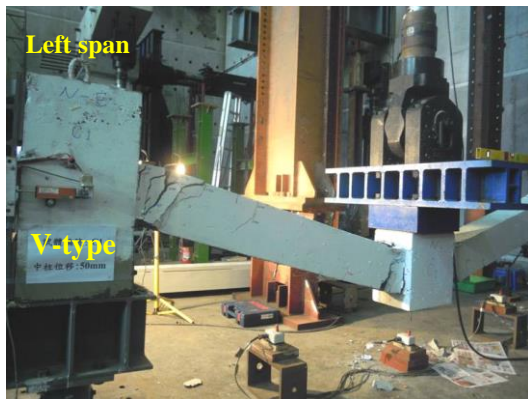

Fig. 4(b) Damage configuration of S2

Fig. 5(a) Damage configuration of *V*-type

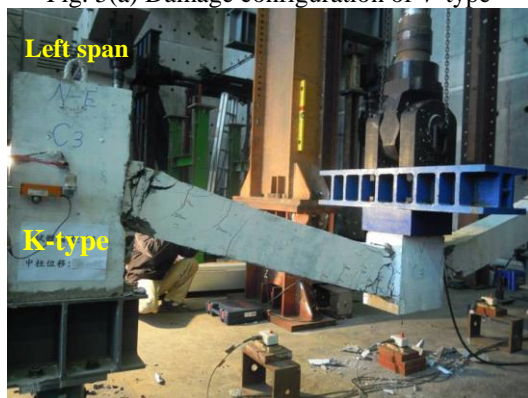Fig. 5(b) Damage configuration of *X*-type

Fig. 5(c) Damage configuration of *K*-type

Fig. 5(d) Damage configuration of *Z*-type

The deformed configurations of the bar-cutoff specimens are presented in Figs. 5(a) - 5(d). It is seen that the flexural cracks induced by positive bending were confined to a smaller region than that by negative bending for the *V*-type specimen, as shown in Fig. 5(a). Due to the cutoff pattern, it had unequal amounts of positive and negative bars. The amount of tensile reinforcement should have influenced the pattern of crack distribution. This was confirmed from the crack distribution of
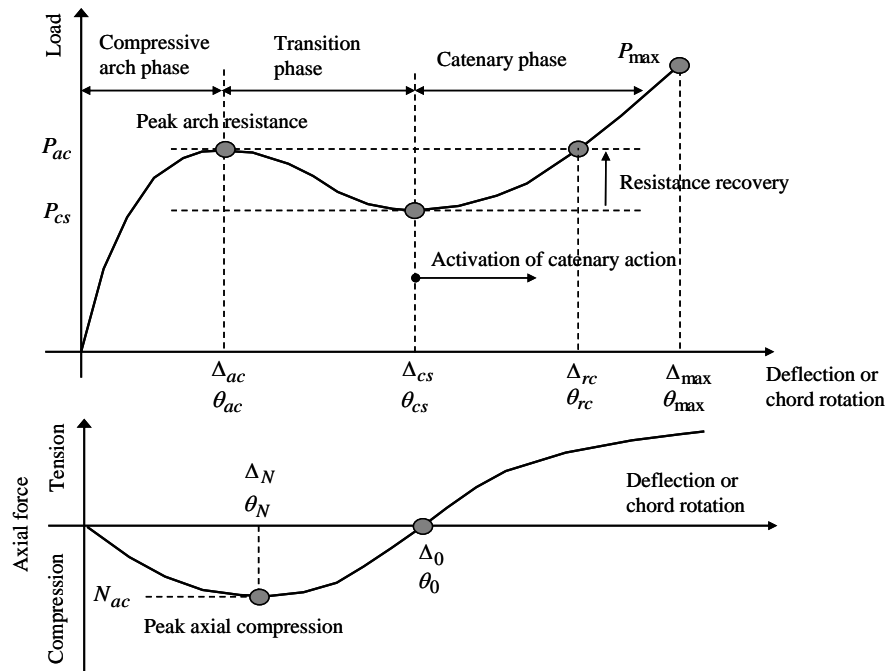
Fig. 6 General definitions of the load-deflection response

the *K*-type specimen in Fig. 5(c). The *K*-type cutoff resulted in a crack pattern similar to the *V*-type at the exterior beam end while a crack pattern similar to S1 at the interior end. For the same reason, similar crack distributions were observed at both beam ends and some flexural cracks formed around the mid-span for the *X*-type specimen, as shown in Fig. 5(b). However, it had more serious horizontal splitting failure than the others at the beam-end region. Perhaps due to accidentally inclined loading surface under large deflection, premature steel fracture happened to the bottom corner bars at the interior beam end of the right span at a displacement of 334 mm. In Fig. 5(d), the *Z*-type specimen presented less apparent horizontal splitting cracks at the beam ends and some obvious vertical cracks formed at the mid-span as the deflection increased beyond 450 mm.

The above observations indicate that the damage and crack patterns of the two-span beams were correlated with the amount of tensile reinforcement and cutoff patterns. Less reinforcement ratios led to more discrete flexural cracks amid the spans. Beam ends with continuous tensile reinforcement presented cracks localized at the beam-end region. Instead, as the tensile bars were cutoff, flexural cracks were originated from the beam ends and propagated towards the cutoff point in the span.

4.2 Structural response

4.2.1 General definitions

In general, three different phases can be defined for the gravitational load-deflection response of a restrained RC beam (Guice and Rhomberg 1989), as shown in the upper plot of Fig. 6. The first one is compressive arch phase, which ranges from the start of the response curve to the peak
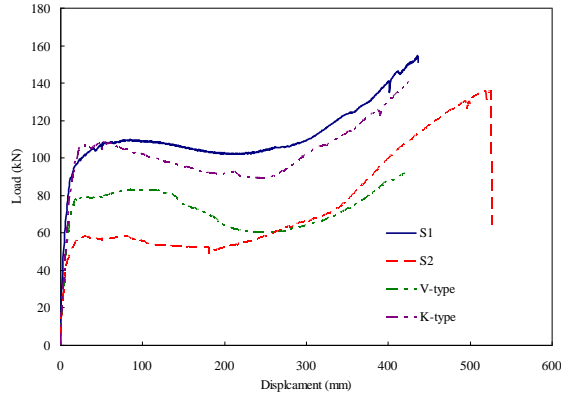
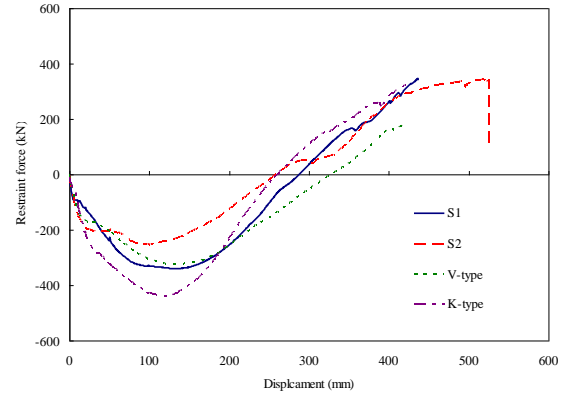Fig. 7(a) Load-deflection responses of the S1, S2, *V*-, and *K*-type specimens

Fig. 7(b) Horizontal restraint force of the S1, S2, *V*-, and *K*-type specimens

arch resistance, P_{ac}. After that, the load response may gradually decrease to P_{cs}, where the catenary action is activated. This range is defined as transition phase, which is followed by the catenary phase. The load resistance may increase during the catenary phase until any of the steel bars fails in rupture. As indicated in the figure, the arch resistance may be restored in the catenary phase. However, it depends on the reinforcement ratio, span-to-depth ratio, and rotational capacity of beam ends. Due to the end restraint, axial force of the RC beam may vary during the gravitational loading history. As demonstrated in the lower plot of Fig. 6, axial compression is induced at the beginning and generally increases to a peak value. Then, it reduces with further deformation and eventually turns into axial tension under large deflection. Some critical deflections and chord rotations are respectively designated as Δ and θ with appropriate subscripts for the convenience of later discussion.

4.2.2 Load and deflection

Fig. 7(a) presents the load-deflection responses of the S1, S2, *V*-, and *K*-type specimens. It is observed that the load-deflection response of the *V*-type specimen lay between S1 and S2 with a similar variation trend in the arch phase. However, it started to descend in the transition phase and eventually became approximately consistent with S2 in the catenary phase. This revealed that those terminated bars of the *V*-type specimen had little contribution to the catenary action. Their corresponding horizontal restraint forces are shown in Fig. 7(b), where negative and positive values respectively represent axial compression and tension of the two-span beams. The compressive bars at the interior beam ends of the *V*-type specimen should have a certain contribution to the arch action such that it had larger compressive restraint force than S2. Meanwhile, because of unequal moment strength, plastic hinges should have appeared at the interior beam ends first for the *V*-type specimen. Thus, the two-span beams would perform as two cantilevers interconnected at the free ends after the interior beam ends had yielded. This cantilever-like behavior would increase the arch action and reduce the catenary action such that the *V*-type specimen had larger compressive and less tensile restraint force less than S2. As the *V*-type cutoff was modified into *K*-type, an improved load-deflection response was obtained. It is seen that the *K*-type and S1 specimens had similar arch and catenary responses. This indicates that the *K*-type cutoff had minor influence on the collapse resistance of the two-span beams.
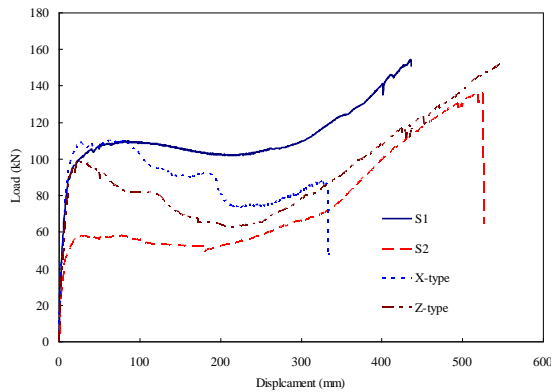
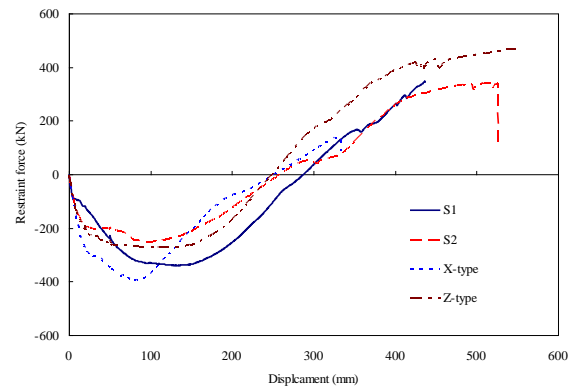Fig. 8(a) Load-deflection responses of the S1, S2, *X*-, and *Z*-type specimens

Fig. 8(b) Horizontal restraint force of the S1, S2, *X*-, and *Z*-type specimens

The load-deflection responses of the *X*- and *Z*-type specimens are compared with that of S1 and S2 in Fig. 8(a). It is observed that S1, *X*-, and *Z*-type specimens had approximately consistent responses at the beginning of the loading process. However, the load resistance of the *Z*- and *X*-type specimens started to degrade at around 10 mm and 90 mm, respectively. The *X*-type specimen displayed a more similar arch resistance to S1. Since the only difference between these two cutoff patterns was the compressive bars at the beam ends, this indicated that the terminated compressive bars of the *X*-type specimen should have contributed to the collapse resistance in the arch phase. In Fig. 8(b), the peak compressive restraint force of S1 and S2 were approximately equal to that of the *X*- and *Z*-type specimens, respectively. This reveals that more compressive bars may result in larger compressive restraint force. In fact, the *X*-type specimen presented similar response to *K*-type up to a deflection of 194 mm, beyond which the load response of *X*-type suddenly dropped towards the *Z*-type response due to serious horizontal splitting failure. Also, similar catenary response was observed for the *X*- and *Z*-type cutoff although the former failed earlier in bar fracture, as shown in Fig. 8(a). Apparently, the terminated compressive bars of the *X*-type specimen had trivial contribution to the catenary resistance. Nevertheless, a comparison of the *X*- and *Z*-type response could confirm that the terminated compressive bars may help to increase the arch resistance.

Contribution of the arch and catenary action to the collapse resistance of the two-span beam may be influenced by the boundary condition of the sub-assemblage. As revealed by Yu and Tian (2013), larger rotational restraint may increase the arch resistance of the two-span beam. However, it has less significant influence on the catenary action. In the experiment, the rotation of the exterior beam-column joint of the left span was monitored with an inclinometer. The joint rotation was generally smaller than 0.003 radians in the arch and transition phases and not larger than 0.006 radians in the catenary phase. Hence, the joint rotation was effectively prevented in the test setup.

4.3 Strain response

Strain gauges were attached to the four corner bars of the left span at the locations of 200 mm, 800 mm, and 1400 mm from the column face, as shown in Fig. 2. The three locations were

respectively corresponding to the exterior end, mid-span, and interior end of the two-span beams. Unfortunately, most of them were damaged during concrete casting or loading process. Only limited gauges attached to the bottom corner bars at the exterior beam end and mid-span had enough data to make a comparison for different bar cutoff. Also, only the Z-type specimen had more survived gauges to investigate strain variation along the span.

Fig. 9(a) show the strain variation of the bottom corner bars at the exterior beam ends. Strain data of the X-type specimen was not obtained because of channel failure. It is seen that the compressive strain at the beam end increased with deflection up to a maximum and then generally decreased with further deformation. Eventually, except for the V-type specimen, those compressive steel bars started to sustain tension under the catenary action. Also, in accordance with Figs. 7(b) and 8(b), larger compressive strain was induced for specimens with larger restraint force except for the S2 and V-type specimens. Because of the cantilever-like plastic behavior as discussed earlier, larger compressive strain was induced for the V-type specimen as compared with others. For the same reason, its compressive bars were still under compression even in the catenary phase. These evidences shows that the V-type cutoff led to less significant catenary action due to the earlier yielding of the interior beam ends. As for the S2 specimen, since it was designed with a smaller tensile reinforcement ratio, its sectional compression depth after concrete crack would be less than other specimens. Therefore, larger compressive strain could be induced under similar compressive restraint force.

Fig. 9(b) shows the strain variation of the bottom corner bars at the mid-span. It is seen that the compressive strain magnitude was comparatively small before entering the catenary phase. The mid-span could be thus regarded as the contraflexural point to estimate the sectional moment for most of the specimens. Figs. 10(a) and 10(b) show the strain variation of the top and bottom corner bars along the left span of the Z-type specimen under five different deflections, respectively. The first deflection was corresponding to the flexural yield load of the specimen, as shown in Table 2. It was obtained from

$$P_y = 2(M_y^- + M_y^+)/L_n \tag{1}$$

where L_n was the clear span length. The second one corresponded to the maximum arch resistance. The third deflection was equal to half the section depth and the fourth one corresponded to the commencement of catenary phase. It is observed that the steel strain at the beam-end regions generally increased up to a deflection equal to half the section depth. After that, perhaps due to partial debonding between the steel bars and surrounding concrete, the strain values moderately decreased. As the deflection was further increased to 400 mm, all the strain values became positive under the catenary action.

4.4 Section forces

Considering the symmetry of beam-end moment strength and the aforementioned strain response, a contraflexural point was assumed at the mid-span for all specimens except the V-type, for which the contraflexural point was assumed at one-third span from the mid-column face. Based on an approximate deformed geometry as shown in Fig. 11, the axial force (T) and sectional moment (M) at the interior beam end were obtained from

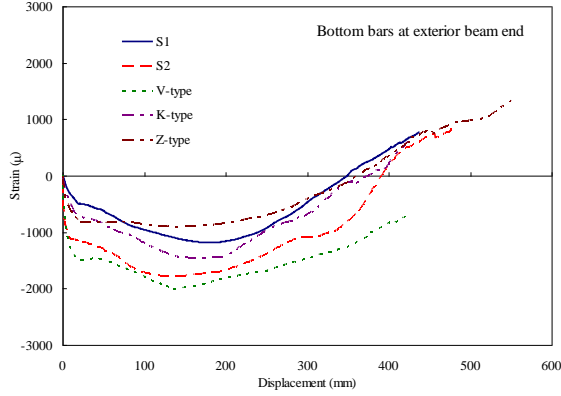$$T = R_H \cos\theta_c + R_V \sin\theta_c \tag{2}$$

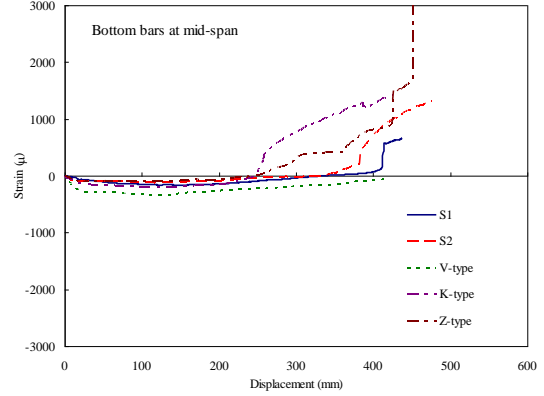Fig. 9(a) Strain variation of the bottom corner bars at the exterior beam ends

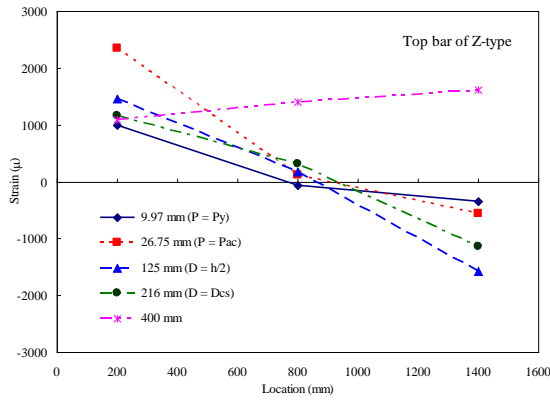Fig. 9(b) Strain variation of the bottom corner bars at the mid-span

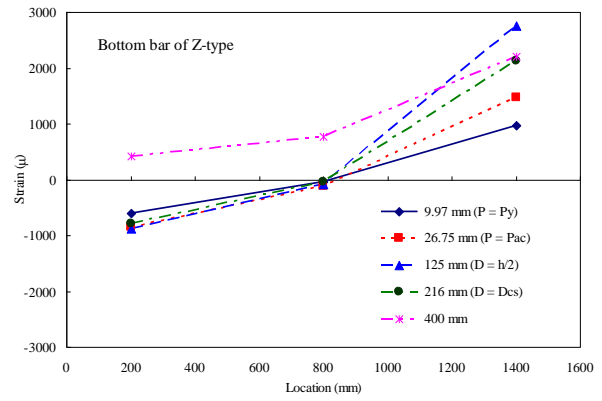Fig. 10(a) Strain distribution along the top bars of the Z-type specimen

Fig. 10(b) Strain distribution along the bottom bars of the Z-type specimen

and

$$M = R_V L_S \cos\theta_c - R_H L_S \sin\theta_c \tag{3}$$

where R_H and R_V were respectively the horizontal and vertical reactions of the sub-assemblage. θ_c was the chord rotation defined as $\theta_c = \Delta/L_n$, in which Δ was equal to the deflection of the interior joint. Also, L_s was equal to $L_n/3$ for the V-type specimen and $L_n/2$ for the others. Then, axial compression was normalized by the nominal compressive strength of the section expressed as

$$N_c = 0.85 f_c'[A_s - (A_s + A_s')] + \sigma_y(A_s + A_s') \tag{4}$$

where A_g, A_s, and A_g' were the area of the gross section, tensile steel, and compressive steel, respectively. σ_y was the yield stress of steel and f_c' was the compressive strength of concrete. Meanwhile, it was observed that the terminated compressive bars had little contribution to the catenary action. Thus, axial tension was normalized by
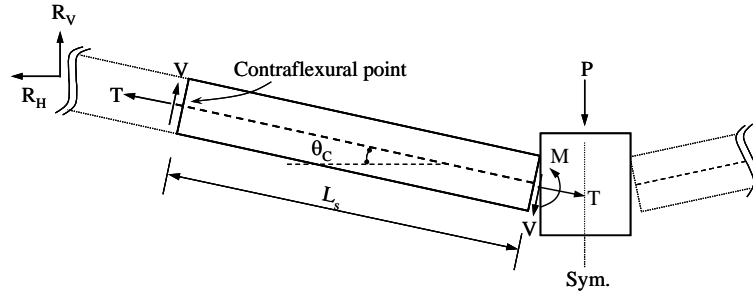
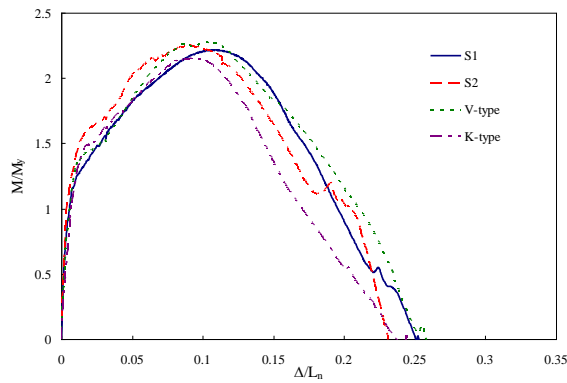Fig. 11 The deformed configuration for calculation of sectional forces

Fig. 12(a) Normalized moments of the S1, S2, V-, and *K*-type specimens
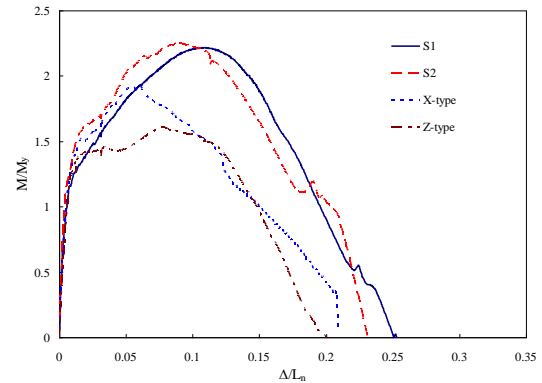

Fig. 12(b) Normalized moments of the S1, S2, X-, and *Z*-type specimens

$$N_t = \sigma_y (A_s + A'_{cs}) \tag{5}$$

where A_s and A'_{cs} were the area of the tensile and continuous compressive steel at the interior beam end, respectively. In addition, the sectional moments were normalized by their corresponding yield moments listed in Table 2.

Figs. 12(a) and 12(b) show the variation of normalized moments (M/M_y) with the chord rotation (Δ/L_n). It is seen that the ratios of M/M_y were larger than 1.0 under the arch action. Eq. (3) reveals that the sectional moment may be increased during the compressive arch phase, i.e., $R_H<0$, and decreased in the catenary phase, i.e., $R_H> 0$. This coincides with basic flexural-axial interaction diagrams in which the moment strength increases with axial compression under tension failure. Most specimens had similar variation and the sectional moments started to deteriorate as the rotation exceeded 0.10 radians, which was close to the acceptance limit in the analysis guidelines issued by the US General Service Administration (GSA 2003). The *X*-type specimen presented earlier decay of sectional moment than the others because of premature bar fracture. Also, the *Z*-type cutoff resulted in a smaller enhancement of moment capacity due to its relatively larger flexural strength but similar compressive arch force as compared with S2.

Figs. 13(a) and 13(b) show the variation of the normalized axial forces (T/N_c or T/N_t) with Δ/L_n. It is observed that the peak axial compression was attained around a rotation of 0.08 radians, which approximately corresponded to half the section depth. The *K*-type specimen had the
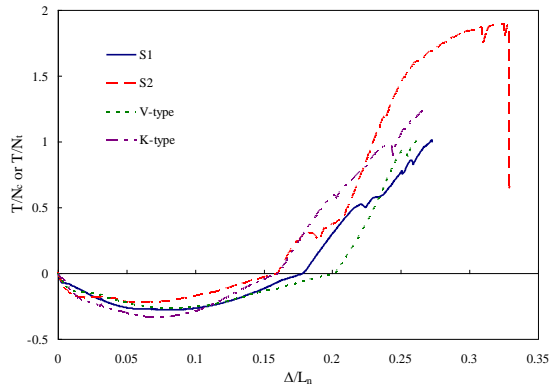
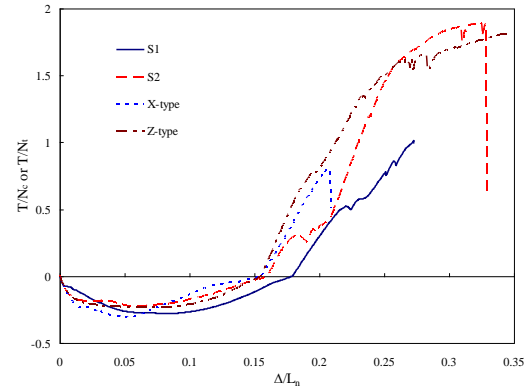Fig. 13(a) Normalized axial forces of the S1, S2, V-, and K-type specimens

Fig. 13(b) Normalized axial forces of the S1, S2, X-, and Z-type specimens

smallest normalized peak axial compression equal to −0.37 and S2 had the largest one equal to −0.22. The axial force changed from compression to tension at a rotation around 0.15~0.17 radians, which approximately corresponded to the section depth. As shown in Fig. 13(a), the axial tension of the *V*- and *K*-type specimens increased at a rate similar to that of S2 and S1, respectively. This reflected their approximate load-deflection responses in the catenary phase, as discussed in Section 4.2. The same phenomenon was observed for the *X*- and *Z*-type specimens. Also, all specimens showed a maximum T/N_t ratio not less than 1.0 except for the *X*-type. This indicates that the axial tension calculated by using Eq. (5) may be regarded as a conservative estimation for the catenary force available in the two-span beams.

5. Bar-cutoff effect and practical considerations

5.1 Comparison of bar-cutoff effect

Normalized load-deflection responses at the peak arch resistance, end of transition phase, strength recovery point, and achieved maximum catenary resistance, as indicated in Fig. 6, were summarized in Table 3 and used to evaluate the effect of bar cutoff. The load resistance was normalized by the flexural yield load obtained from Eq. (1) to inspect strength enhancement in the arch and catenary phases. At first, it is seen that the influence of bar cutoff on strength enhancement at the peak arch resistance was not significant. With a lower tensile reinforcement ratio, the S2 specimen had a moderate larger strength enhancement than the others. The *Z*-type specimen achieved the peak arch resistance earlier than the other bar-cutoff specimens. Even so, all of them came to similar chord rotations at the end of the transition phase. The *V*-, *X*-, and *Z*-type cutoff resulted in significant strength degradation in the transition phase. The normalized resistance even dropped to less than 1.0 for the latter two specimens. It is noted that the *X*- and *Z*-type specimens shared a distinct characteristic from the others in that 50% of their top and bottom bars were terminated simultaneously at the mid-span region. This could be the reason for their serious strength degradation. The *K*-type cutoff resulted in less strength degradation than the others.

Table 3 Normalized loading resistances and chord rotations

Specimen	P_{ac}/P_y	θ_{ac}	P_{cs}/P_y	θ_{cs}	θ_{rc}	P_{max}/P_y	θ_{max}
S1	1.39	5.38%	1.29	13.34%	22.63%	1.96	27.25%
S2	1.43	4.84%	1.20	11.34%	19.19%	3.34	32.38%
V-type	1.42	5.37%	1.02	15.06%	24.16%	1.56	26.25%
X-type	1.40	3.72%	0.93	13.88%	Not available	1.12	20.50%
K-type	1.39	3.41%	1.13	14.94%	23.69%	1.79	26.56%
Z-type	1.30	1.68%	0.82	13.51%	23.13%	2.02	34.42%

Recovery of the peak arch resistance is an important subject in the evaluation of catenary action. As observed from Table 3, except the *X*-type specimen, the arch resistance of the other three bar-cutoff specimens could be recovered at similar chord rotations. The S2 specimen showed an earliest strength recovery at θ_{rc}=19.2% due to its lowest tensile reinforcement ratio. The specimens with bar cutoff presented a delayed recovery of arch resistance. Moreover, most pronounced strength enhancement in the catenary phase was observed for the S2 specimen. Because of bar cutoff and increased tensile reinforcement ratio, the *Z*-type specimen displayed less pronounced strength enhancement than S2 under similar chord rotations. In fact, if estimated at the chord rotation of 26.25%, the P_{max}/P_y ratio of the *Z*-type specimen was around 1.52, which was approximately equal to that of the *V*-type. This confirms the earlier observation from the test results that the terminated compressive bars had minor effect on the catenary resistance. Nonetheless, they could help to preserve the arch resistance and thus mitigate the strength degradation in the transition phases.

Similar comparisons were obtained that the *Z*-type specimen had approximately equal strength enhancement to the *X*-type specimen if evaluated at the same rotation of 20.5%. It is inferred that the *X*-type specimen could have similar catenary response to the *Z*-type if the premature bar fracture did not happen. Also, strength enhancement of the *X*-type specimen was only slightly less than that of the *V*-type at the same chord rotation. Overall speaking, the K-type cutoff resulted in better resistant performance than the others. The *V*-type and *Z*-type could have similar strength enhancement in the catenary phase. However, more significant strength degradation occurred in the transition phase for the *Z*-type specimen.

5.2 Practical considerations

The ACI design code has specified detailed regulations for structural integrity consideration in Chapter 7.13 (ACI 2011). All the test specimens satisfied the code requirements. The *X*-, *K*-, and *Z*-type specimens had approximately the same beam-end yield moments as S1. However, due to different bar cutoff, they presented distinct load-deflection responses under the gravitational loading. For efficient development of catenary resistance, it is preferred that there is no bar cutoff in the two-span beams bridging over the column prone to sudden failure. However, if bar cutoff is inevitable at the mid-span region, it is suggested to extend the steel bars at least over the mid-span before cutoff. Also, to mitigate strength degradation in the transition phase, simultaneous cutoff of top and bottom bars in the mid-span region is not recommended. For the *V*-type cutoff, which is conventionally dominated by gravitational design, it can be replaced with the *K*-type layout to increase the progressive collapse resistance. For the *X*-type layout in general seismic-controlled

design, it is suggested to extend the terminated bottom bars over the mid-span for resembling the *K*-type response under column loss.

The progressive collapse analysis guidelines issued by the US General Service Administration (GSA 2003) suggest an acceptance rotation of 0.105 radians for RC beams, which is less than the values of θ_{cs} in Table 3. Also, it is observed from Figs. 12(a) and 12(b) that the maximum moments were generally developed at a rotation larger than 0.063 radians, which is the maximum acceptable rotation for RC beams recommended by the UFC 4-023-3 guidelines (DoD 2009). These indicate that both guidelines neglect the contribution of catenary action to the collapse resistance of flexural RC members and thus are conservative for practical applications.

6. Conclusions

An experimental study was carried out to investigate the column-loss response of RC beam-column sub-assemblages designed with different bar-cutoff patterns. According to the bar layout, *V*-, *X*-, *K*-, and *Z*-type cutoff were defined to compare with two benchmark specimens, S1 and S2, which were designed with continuous main reinforcement. Experimental results indicated that those specimens (S1, *X*-, *K*-, and *Z*-type) with approximately equal moment strength at the beam ends had similar peak arch resistance but varied strength degradation in the transition phase. The *X*-type specimen presented moderately larger arch resistance and less strength degradation than the *Z*-type. This revealed that the compressive bars (i.e., bars under compression at the beam ends) terminated at one-third span should have helped to preserve the arch resistance and mitigate strength degradation. However, these terminated compressive bars had minor influence on the catenary response. Therefore, their contribution may be neglected in the estimation of catenary force. Similarly, as compared with the S2 specimen, test results of the *V*-type cutoff implied that its terminated bars (i.e., top bars at beam ends and bottom bars at mid-span) did not really participate in the development of catenary action. Hence, the available catenary force may be conservatively estimated as the product of the steel yield stress and the areas of beam-end tensile and continuous compressive reinforcement.

Investigation of the bar-cutoff effect indicated that those four types of bar cutoff had similar strength enhancement around 30%~40% at the peak arch resistance. Although the strength enhancement decreased in the transition phase, the peak arch resistance could be recovered in the catenary phase except the *X*-type specimen, to which premature bar fracture had occurred. The *K*-type specimen had the best strength enhancement among all the cutoff patterns and presented approximately consistent response with S1. Thus, the *K*-type cutoff is preferred in the progressive collapse resistance design as bar cutoff is inevitable. For the two-span beams bridging over a frame column vulnerable to sudden failure, the steel bars had better be extended at least over the mid-span before cutoff. For the conventional *V*-type cutoff dominated by gravitational design, it can be replaced with the *K*-type by extending the terminated bottom bars into the mid-column joint. For the *X*-type cutoff in general seismic-controlled design, the terminated bottom bars can be extended over the mid-span for resembling the *K*-type response under column loss. The test results of this study were focused on the progressive collapse resistance before bar fracture. Further experimental investigation may be needed for clarifying the post-fracture response under the gravitational loading.

Acknowledgements

References

Abruzzo, J., Matta, A. and Panariello, G. (2006), "Study of mitigation strategies for progressive collapse of a reinforced concrete commercial building", *J. Perform. Constr. Facil.*, **20**(4), 384-390.

ACI (2011), *Building code requirements for structural concrete, Standard ACI 318-11*, American Concrete Institute, Farmington Hills, Michigan, USA.

Almusallam, T.H., Elsanadedy, H.M., Abbas, H., Alsayed, S.H. and Al-Salloum, Y.A. (2010), "Progressive collapse analysis of an RC building subjected to blast loads", *Struct. Eng. Mech.*, **36**(3), 301-309.

Choi, H. and Kim, J. (2011), "Progressive collapse-resisting capacity of RC beam-column sub-assemblage", *Mag. Concrete Res.*, **63**(4), 297-310.

DoD (2009), *Unified facilities criteria: design of buildings to resist progressive collapse, UFC 4-023-03*, Department of Defense, Washington DC, USA.

Ellingwood, B.R. (2006), "Mitigating risk from abnormal loads and progressive collapse", *J. Perform. Constr. Facil.*, **20**(4), 315-323.

GSA (2003), *Progressive collapse analysis and design guidelines for new federal office buildings and major modernization projects*, General Service Administration, Washington DC, USA.

Guice, L.K. and Phomberg, E.J. (1989), "An analogous model for slabs using a truss element", *Comput. Struct.*, **31**(5), 767-774.

Izzuddin, B.A. (2005), "A simplified model for axially restrained beams subjected to extreme loading", *Steel Struct.*, **5,** 421-429.

Kim, J. and An, D. (2009), "Evaluation of progressive collapse potential of steel moment frames considering catenary action", *Struct. Des. Tall Spec. Build.*, **18**(5), 455-465.

Lee, C.H., Kim, S., Han, K.H. and Lee, K. (2009), "Simplified nonlinear progressive collapse analysis of welded steel moment frames", *J. Constr. Steel Res.*, **65**(5), 1130-1137.

Liu, J.L. (2010), "Preventing progressive collapse through strengthening beam-to-column connection, Part 1: theoretical analysis", *J. Constr. Steel Res.*, **66**(2), 229-237.

Mohamed, O.A. (2006), "Progressive collapse of structures: annotated bibliography and comparison of codes and standards", *J. Perform. Constr. Facil.*, **20**(4), 418-425.

Nair, R.S. (2006), "Preventing disproportionate collapse", *J. Perform. Constr. Facil.*, **20**(4), 309-314.

Sadek, F., Main, J.A., Lew, H.S. and Bao, Y. (2011), "Testing and analysis of steel and concrete beam-column assemblies under a column removal scenario", *J. Struct. Eng.*, **137**(9), 881-892.

Sasani, M. and Kropelnicki, J. (2008), "Progressive collapse analysis of an RC structure", *Struct. Des. Tall Spec. Build.*, **17**(4), 757-771.

Sasani, M. and Sagiroglu, S. (2010), "Gravity load redistribution and progressive collapse resistance of 20-story reinforced concrete structure following loss of interior column", *ACI Struct. J.*, **107**(6), 636-644.

Sasani, M., Werner, A. and Kazemi, A. (2011), "Bar fracture modeling in progressive collapse analysis of reinforced concrete structures", *Eng. Struct.*, **33**(2), 401-409.

Su, Y., Tian, Y. and Song, X. (2009), "Progressive collapse resistance of axially-restrained frame beams", *ACI Struct. J.*, **106**(5), 600-607.

Tian, Y. and Su, Y. (2011), "Dynamic response of reinforced concrete beams following instantaneous removal of a bearing column", *Int. J. Concrete Struct. Mater.*, **5**(1), 19-28.

Tsai, M.H. and Huang, T.C. (2013), "Progressive collapse analysis of an RC building with exterior partially

infilled walls", *Struct. Des. Tall Spec. Build.*, **22**(4), 327-348.

Yagob, O., Galal, K. and Naumoski, N. (2009), "Progressive collapse of reinforced concrete structures", *Struct. Eng. Mech.*, **32**(6), 771-786.

Yi, W.J., He, Q.F., Xiao, Y. and Kunnath, S.K. (2008), "Experimental study on progressive collapse-resistant behavior of reinforced concrete frame structures", *ACI Struct. J.*, **105**(4), 433-439.

Yu, J. and Tan, K.H. (2013), "Experimental and numerical investigation on progressive collapse resistance of reinforced concrete beam column sub-assemblages", *Eng. Struct.*, **55**, 90-106.